The laser-backscattering equations and their application to the study of the atmospheric structure

R. Castrejón-García
Instituto de Investigaciones Eléctricas
Av. Reforma 113, Col. Palmira, 62490 Temixco, Mor., México.
e-mail: rcg@iie.org.mx

J. R. Varela
Universidad Autónoma Metropolitana-Iztapalapa
Av. Michoacán y la Purísima, Col. Vicentina, 09340, México, D. F.
e-mail: jrvh@xanum.uam.mx

J. R. Castrejón-Pita
Centro de Investigación en Energía, Universidad Nacional Autónoma de México
Apdo. Post. 34, Temixco, Mor., 62580, México.
e-mail: jrcp@cie.unam.mx

A. Morales
Centro de Ciencias Físicas, Universidad Nacional Autónoma de México
Apdo. Post. 48-3, Cuernavaca, Mor., 62251, México.
e-mail: mori@fis.unam.mx

Recibido el 19 de marzo de 2002; aceptado el 8 de julio de 2002

In this work a method for interpreting backscattering signals acquired by a lidar is described. The method is based on the elastic scattering of laser radiation due to gases and particles suspended in the atmosphere (bulk effects). We propose a space-time diagram which helps to evaluate the arguments of the equation that serves to calculate the lidar signal in terms of the backscattering coefficient. We describe how the system detects gradients on this coefficient, along the laser optical path. To illustrate the method, we present some typical lidar results obtained in the neighborhood of Mexico City.

Keywords: Lidar; atmospheric light-backscattering; laser remote sensing.

En este trabajo se describe el desarrollo de un método que sirve para interpretar las señales de retrodispersión adquiridas por un sistema similar al radar conocido como lidar. El método se basa en la dispersión elástica de radiación láser, producida por gases y partículas suspendidas en la atmósfera (efecto global). Presentamos un diagrama de espacio-tiempo que ayuda a evaluar los argumentos de la ecuación que permite calcular la señal lidar en términos del coeficiente de retrodispersión. Explicamos también, el procedimiento que permite detectar los gradientes de ese coeficiente a lo largo de la trayectoria óptica láser. Se muestran algunos resultados de la aplicación del método en sitios vecinos a la Ciudad de México.

Descriptores: Lidar; retrodispersión atmosférica de luz; detección remota con láser.

PACS: 42.68.Wt

1. Introduction

In recent years, the surveillance and control of atmospheric pollution have acquired special relevance. In order to know the relation between pollution and its effects, it is necessary to count on reliable and appropriate measuring systems that can solve the large spatial and temporal variation of the presence and distribution of pollutants.

The advantages of a suitable measuring system in addition to providing useful information to establish data bases for studies on air pollution, can serve to establish criteria on the effectiveness of the procedures and to evaluate the effect of the strategies implanted to its diminution. Likewise, it can serves to know if the settlement of some new industry or the increase of the traffic of vehicles rebound in the already existing levels of pollution and to plan the urban and industrial growth based in the knowledge of pollution levels.

The traditional equipment and techniques for measurement of pollutants display results obtained in a certain position and accumulated in a certain period, which provides local information on the measurement place, but not its distribution and impact in the neighboring zones and surroundings.

Three decades ago, with the incoming of the laser, the world has witnessed its particular evolution and application to the study of the atmosphere. In fact, the atmosphere was one of the first sites where the properties of the laser light (high power, monochromaticity, short pulse duration and collimation), were put on trial. With the invention of ruby lasers, generators of powerful optical pulses in the year of 1962 [1], the use of the laser in remote optical probing was made possible. Fiocco and Smullin [2], and Ligda [3], who in 1963,

registered echoes of the laser light pulse from the troposphere and the upper regions of the atmosphere, carried out the earlier studies of the atmosphere with laser. That was the origin of the lidar (an acronym for light detection and ranging).

With these new remote sensing technologies based on laser sources, analysis of the atmosphere can be made in large areas and in short periods of time, even at long distances and inaccessible places. This new technology has proved its wide application in the evaluation of the structure, properties and composition of the atmosphere.

Nowadays, the application of lidar in the study of the atmosphere is made every time most frequently. In diverse parts of the world [4] high specialized lidars are satisfactorily used in: the determination of the vertical profile of aerosol concentrations [5], in the study of the nocturnal radiation inversion [6], in the design of atmospheric monitoring networks [7], in the determination of the atmospheric boundary layer height [8, 9] and in the study of the characteristics and dispersion parameters of chimney plumes [10–15].

The impact of this relatively new tool has been such, that in some countries its use and application have begun to be adopted by institutions dedicated to environmental protection as a standardized method for the study of pollution plumes in the atmosphere [16].

The interest in this work is to develop a numerical procedure that highlights the gradients of the atmosphere backscattering properties. To that end, in section 3 a space-time diagram is applied to the classic equations that describe the backscattering of a laser pulse by gases and particles in atmosphere. In section 4, the study of real cases is presented.

2. The lidar

In a general scheme, a lidar can be classified in accordance with the interaction that the laser light suffers with the atmosphere in two kinds: elastic scattering lidar and inelastic scattering lidar. In the first kind, the phenomena in which the laser radiation is scattered by atoms, molecules, aerosols or particles in the air, without undergoing change in its wavelength (or frequency) are included. In inelastic scattering, a change in the wavelength of the scattered radiation exists, that is to say, the frequency (or energy) of the incident photon is different from the frequency of the scattered photon. Here, within these techniques, the Raman scattering lidar and the fluorescence lidar can be mentioned.

In elastic scattering, the physical size of the particle determines the type of scattering. If the particles are atoms or molecules (*i.e.* a gas or mixture of gases) the scattering is known as Rayleigh scattering, due to the name of the involved theory [17]. If the sizes of the particles (airborne particulates or aerosols) are comparable to that of the laser wavelength, then the scattering is called Mie scattering. In an elastic scattering lidar the analysis of the received signal is made taking into account these two types of scattering.

An elastic lidar does not detect, through elastic scattering, the presence of a compound or chemical species individually; but the bulk scattering produced in joint by the presence of gases, compounds, particles and aerosols in the atmosphere. This allows to locate, in direction and distance, zones in which changes of the atmospheric structure like: gradients of density, humidity, height of mixing layer, pollutant plumes, etc., exist. In this work only the elastic case is considered.

A typical lidar is illustrated in Fig. 1, its principle of operation is as follows: an intense pulse of luminous energy is produced by the laser and sent, through the output optics, toward the atmosphere. The scattered radiation that returns backward to its origin point (the phenomenon is called backscattering) is collected with the receiving optics (the telescope) and sent through a spectral filter to the detector. The function of the spectral filter is to distinguish the radiation of the laser, from the background radiation (diffuse solar or artificial light at other wavelengths). As in radar, the lidar signal transforms the information from position into time.

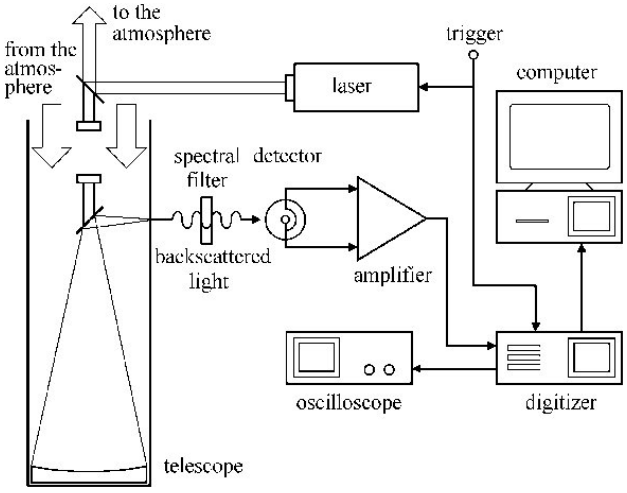

FIGURE 1. Schematic diagram of a lidar.

The signal in the detector is converted into an analog electrical signal that is amplified with a low noise amplifier. This analog signal is transferred to a digitizer, where it is converted into numerical data that can be processed or stored in a computer. The analog signal can also be visualized with an oscilloscope, where the behavior of the received signal is observed. Since the luminous signal is acquired in real time, it must be manipulated with high-speed electronics, due to the rapidity with which the phenomenon is developed.

3. The space-time diagram and the lidar atmospheric backscattering equation

The irradiance S as a function of time t, of the laser pulse produced by a laser located in position $R = 0$, is shown in Fig. 2. As the pulse propagates with speed c, the irradiance is

$$S(t, R) = S\big(t - \frac{R}{c}\big) = S(t - R'), \qquad (1)$$

with $R' = R/c$, the scaled value of R. In terms of the reduced time $t' \equiv t - R'$, the irradiance is

$$S(t, R) = S(t'). \tag{2}$$

Since $t' = t$ in $R' = 0$, $S(t')$ in Eq. (2) is the function represented in Fig. 2. At any other values of R' and t, the same t' characterize the same position in the pulse. The reduced time $t'_1 = t_1 - R'$ is a parameter associated with the irradiance at t_1 in Fig. 2, which is independent of t and R'. Indeed, for a different time t_2, the reduced time is

$$t'_2 = t_2 - [R' + (t_2 - t_1)] = t_1 - R' = t'_1. \tag{3}$$

It is important to note that each position of the pulse in Fig. 2 has a different reduced time.

The representation of a travelling light pulse S in the space R'-t' is shown in Fig. 3. For a fixed value of t, the relation between R' and t' is $R' = -t' + t$; therefore, straight lines in Fig. 3, with slope $m = -1$, are lines of equal time t. P_0 and P_1 are points with the same t' that characterizes the irradiance in point P of the laser pulse S. Two straight lines, one with $t = 0$ and the other with $t = t_1$, show that for $t = 0$ the point P is in $R' = R'_0$, and the same point is in R'_1 at $t = t_1$. As can be seen from the figure, positive t' are delayed in position with respect to negative t'.

Now we show that the space before described is useful to describe a backscattering event. In such event, the velocity changes its sign, therefore points P_1 and P_2 in Fig. 4, change their R' to $-R'$. Then the reduced time after backscattering is $t'' = t + R'$, which in terms of the reduced time before backscattering t', is

$$t'' = t' + 2R'. \tag{4}$$

Equation (4) shows that all points on the straight line

$$R' = -\frac{1}{2}t' + \frac{1}{2}t'', \tag{5}$$

have, after backscattering, the same reduced time t''. Since the same reduced time means same point on the laser pulse, the irradiance of all the points on the line must be added to compose the backscattered pulse, which is the lidar return signal.

In Fig. 4, a laser pulse S of duration τ with $-\tau\ /\ 2 \leq t' \leq \tau\ /\ 2$, interacts with a region of the atmosphere located between R'_1 and R'_2, with a backscattering coefficient represented by the curve $\beta(R')$. The backscattering begins when the laser pulse reaches that region. The points P_1 and P_2 which are, before backscattering, on the bold line with slope $m = -1/2$, described by Eq. (5), are transformed in points P'_1 and P'_2 on the line L, after backscattering. Since both points have the same reduced time t''_1, the lidar signals will reach the detector at the same time t''_1, despite of the fact that the backscattering events in P_1 and P_2 occurred at different times t_1 and t_2, respectively.

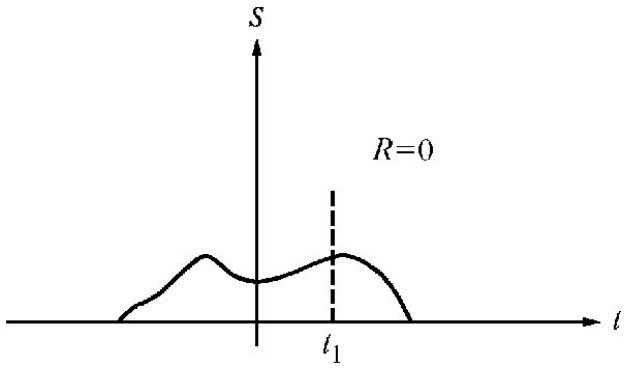

FIGURE 2. Irradiance versus time of laser pulse.

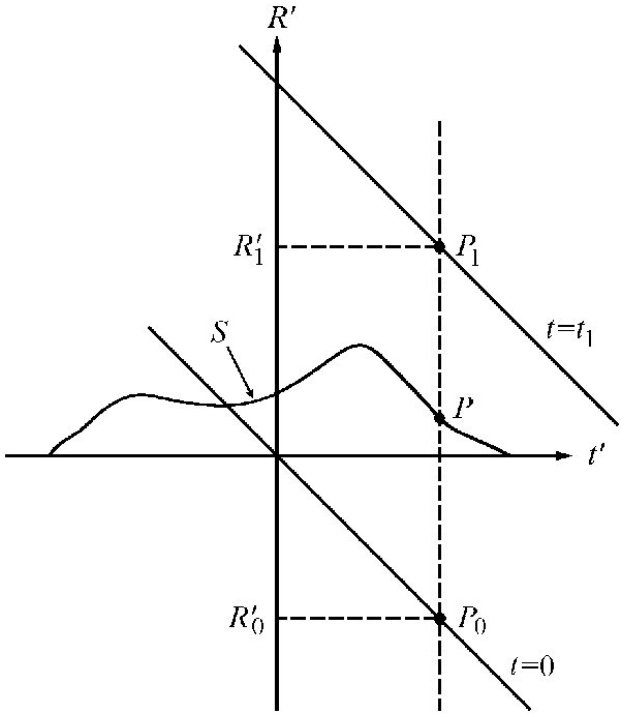

FIGURE 3. A laser pulse in the R'-t' diagram.

In a lidar, in which the source (laser) and the receiving optics (telescope and detector) are located at the same place $R' = 0$, the power of the signal $P(t'')$ at $t = t''$ that receives the detector is given by the addition of the contributions of all points on the bold line of Fig. 4. According to Measures [18], this is expressed as

$$P(t'') = \frac{A_0}{c}\varsigma(\lambda)\int_{R'_1}^{R'_2}\beta(\lambda, R')T_A(\lambda, R') \times \xi(R')I(\lambda, R')A(R')\frac{dR'}{R'^2}, \tag{6}$$

where, A_0 is the area of objective lens or mirror of the receiving optics ; $\varsigma(\lambda)$, is the spectral response of the receiving system (receiving optics, spectral filter and detector); $\beta(\lambda, R')$, represents the Rayleigh-Mie backscattering coefficient associated to the atmosphere element at the laser wavelength λ; $T_A(\lambda, R')$, is the spectral atmospheric transmission coefficient along the path R'; $I(\lambda, R')$, is the laser irradiance at

range R'. A is the area irradiated by the laser at range R'. The factor $1/c^2R'^2$ takes into account the attenuation of the signal with distance assuming that the field of view of collecting optics is bigger than the angle subtend by A; $\xi(R')$, is a geometrical factor that represents the probability that the radiation scattered by the atmosphere will be received by the detector, this factor is the unity when the collecting optics and the laser are coaxial, and the field of view of collecting optics is bigger than the angle subtend by A.

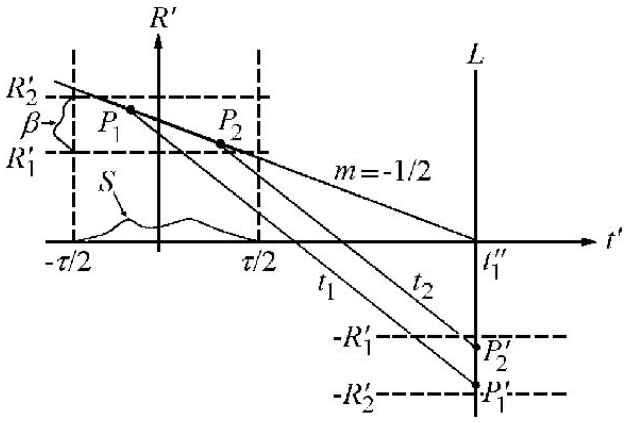

FIGURE 4. A backscattering event in the R'-t' diagram.

The laser irradiance at range R' given by Measures (See Ref. 18), is the irradiance at $R' = 0$ reduced by the atmospheric transmission factor $T(\lambda, R')$, then $I(R') = T(\lambda, R')S(t')$. Introducing R' from Eq. (5), the value of $I(R')$ in Eq. (6), and taking $\xi = 1$, we obtain the lidar signal power:

$$P(t'') = \frac{-A_0}{2c}\varsigma \int_{-\frac{1}{2}t'_1+\frac{1}{2}t''}^{-\frac{1}{2}t'_2+\frac{1}{2}t''} \beta(R')T_A(R') \times T(R')S(t')A(R')\frac{dt'}{R'^2}, \quad (7)$$

where t'_1 and t'_2 are the values of t' at intersections of line with slope $m = -1/2$ with the borders of the interaction rectangle formed by $-\tau/2$, $\tau/2$, R'_1 and R'_2, in Fig. 4.

In a typical lidar the laser output is a pulse of constant irradiance S. Duration of the pulse is τ centered around $t' = 0$. Since in our case, $\tau << R'_2 - R'_1$, the t'-dependent factors can be considered constants over this small interval of integration.

Therefore the integration in Eq. (7) can be approximated as

$$P(t'') = \frac{A_0 S}{2c}\varsigma\beta(R')T_A(R')T(R')A(R')\frac{\tau}{(R')^2}. \quad (8)$$

It is important to observe that Eq. (8) does not change in case $R'_1 = 0$ and $R'_2 = \infty$ because $\tau << R'_2 - R'_1$.

The irradiance $T(R')S$ at R' is

$$T(R')S = \frac{E_L T(R')}{\tau A}, \quad (9)$$

where E_L is the energy of the laser pulse.

For $t' = 0$, Eq. (4) gives $t'' = 2R'$, then introducing TS from Eq. (9) and $t'' = 2R'$ in Eq. (8), we obtain

$$t''^2 P(t'') = \frac{2A_0 E_L}{c}\varsigma\beta(R')T_A(R')T(R'), \quad (10)$$

Equation (10) depicts the atmospheric elastic backscattering and constitutes the basis for the development of the method for the scrutiny of the lidar return signal of an elastic scattering lidar.

According to Beer-Lambert law, the atmospheric transmission factor T_A is

$$T_A(R') = e^{-c\int_0^{R'}\kappa(R')dR'}, \quad (11)$$

where κ is the atmospheric attenuation coefficient.

For elastic scattering $T_A = T$, then Eq. (10) is

$$t''^2 P(t'') = F(R') \equiv \frac{2A_0 E_L}{c}\varsigma\beta(R')e^{-2c\int_0^{R'}\kappa(R')dR'}. \quad (12)$$

The left term of Eq. (12), corresponds to the experimental data obtained by the collecting optics and the electronic timing.

From Eq. (12), we obtain

$$\frac{dF}{F} = \frac{d\beta}{\beta} - 2c\kappa dR', \quad (13)$$

where dF and $d\beta$ are the differentials corresponding to differential dR'. Equation (13) shows that the gradients of F and β aside from a constant factor, only differ by a term proportional to the local value of κ.

4. Experimental results

The following scanning examples were carried out with a lidar consisting of a dye laser with second harmonic generation at a wavelength of 300 nm and a receiving coaxial telescope with 600 mm diameter. The lidar return signals were digitized with a digitizer that furnished a resolution $L = 15$ m. The lidar signals were averaged on 25 laser firings at each direction.

Figure 5 shows a graph of an actual lidar return signal caused by the atmospheric backscattering of the laser pulse. It is a plot of power $P(t'')$, of the received backscattered light, versus distance $R = cR'$; any non-homogeneity in the atmosphere is manifested in intensity, distance and direction. Fig. 6, shows a plot of $F(R') = t''^2 P(t'')$ versus R after corrected to cancel the inverse quadratic dependence, as depicted by Eq. (12). According to Eq. (13) the plot of $F(R')$ shows the same spatial structure as that of β. The distortion term $2c\kappa dR'$ is important only in locations where κ is significantly large. Hence, assuming that the distortion term is negligible, the plot of $F(R')$ provides enough information to display a representation of the structure of the atmosphere, in spite of the lack of knowledge of values β and κ.

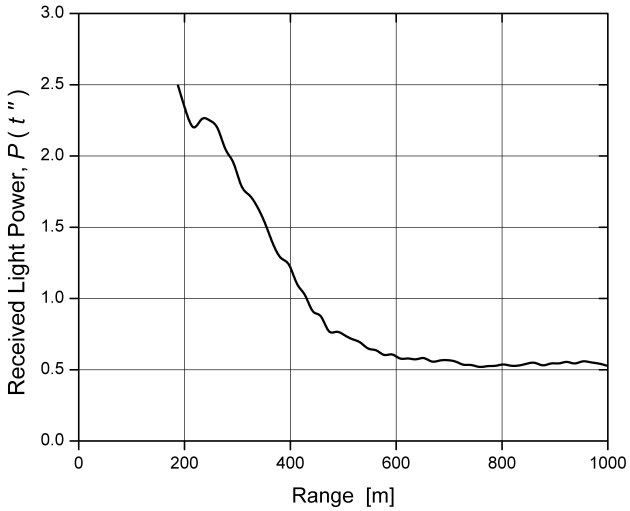

FIGURE 5. A lidar return signal, as backscattered by the atmosphere.

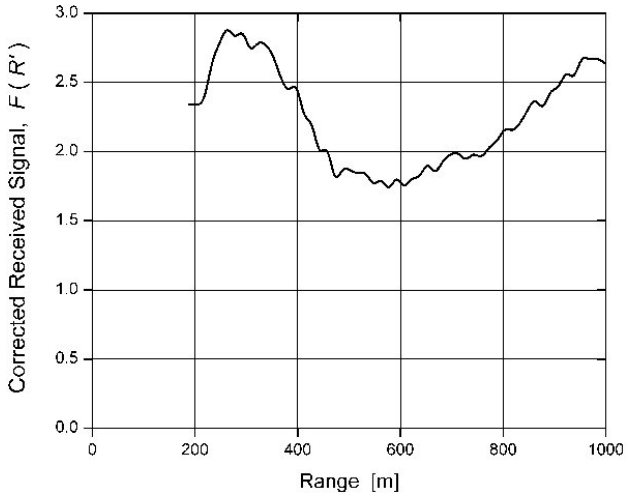

FIGURE 6. Plot of the corrected lidar return signal, as calculated with Eq. (12).

In order to evaluate the performance of the proposed method in determining the gradient of backscattering coefficient and its capability to show the structure of the atmosphere, the raw data obtained with the lidar were processed with Eq. (12), for series of laser shots.

Figure 7 shows a plot of the lidar signal power obtained from an azimuthal scan parallel to ground performed over a 750 MW gas fired power plant in the north of the state of México. The pollutant plume emitted by the plant, its position and its impact area can be clearly appreciated.

Figure 8 shows a plot of a scan performed over the same power plant but the lidar positioned on a southern location. Besides the plume, the dust and pollutants emitted by a heavily vehicle traffic road is appreciated at the right side of the plot.

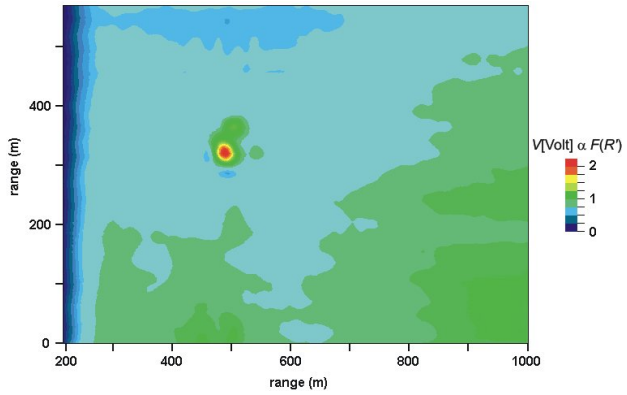

FIGURE 7. Azimuthal lidar scan over a gas fired power station, located north of México City.

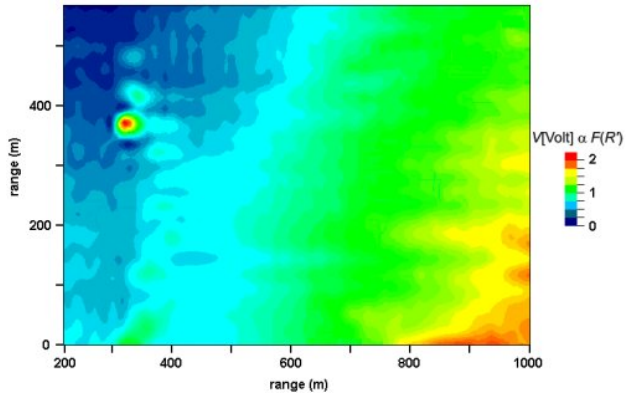

FIGURE 8. Azimuthal scan over same power plant as Fig. 7, on a southern location.

Figure 9 shows a plot of a long range azimuthal scan (3 km) performed over a power complex composed by a 1500 MW fuel oil power plant and an oil refinery, located at the south of the state of Hidalgo. The contribution of both can be observed in the figure. The refinery is located at the lower part of the graph while the plumes emitted by the power plant facility are clearly located at the middle part of the plot. It is also interesting to observe that there is a difference in magnitude (color bar) between the emissions of a fuel-oil power plant and a gas powered plant in Fig. 7.

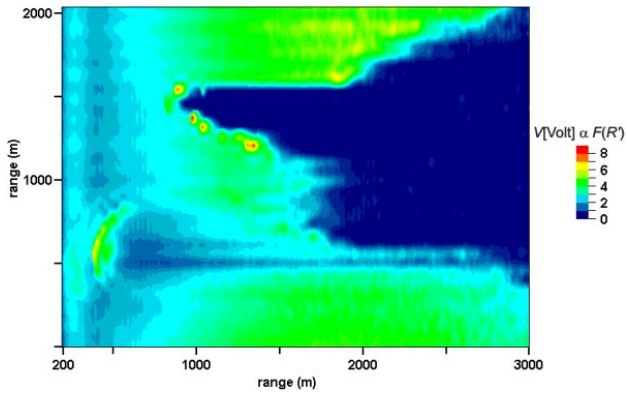

FIGURE 9. Azimuthal scan over an industrial power complex at Hidalgo state

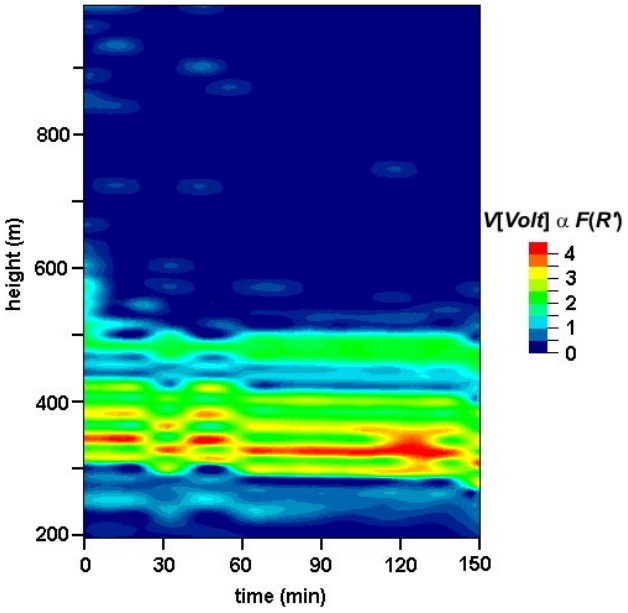

FIGURE 10. Time domain zenithal lidar probing at México City.

Figure 10 is a time domain plot, obtained with vertical laser firings, which shows the zenithal profile of the atmosphere structure. The different layers of the atmosphere and its temporal evolution can be clearly observed in the figure. The experimental data were obtained in a location inside the metropolitan area of Mexico City during a thermal inversion episode.

5. Conclusion

In this work, a space-time diagram that serves to interpret the return lidar signal obtained with a laser has been proposed. The diagram was used in the equations to describe the operation of a lidar based on the atmospheric elastic backscattering. This method displays the details of the atmosphere structure and has been applied and tested with satisfactory results, for several locations around central México.

Acknowledgements

R. C. G. expresses his gratitude to the Universidad Autónoma Metropolitana-Iztapalapa for providing him its intellectual atmosphere. This research was supported by the Consejo Nacional de Ciencia y Tecnología and the Instituto de Investigaciones Eléctricas and the DGAPA–UNAM (IN101100), México.

1. McClung, F. J. and R. W. Hellwarth, *Giant Optical Pulsations from Ruby, J. Appl. Phys.* **33** (1962) 828.
2. Fiocco, G. and L. D. Smullin, *Detection of Scattering Layers in the Upper Atmosphere (60-140 km) by Optical Radar, Nature.* **199** (1963) 1275.
3. Ligda, M. G. H., *Proc. Conf. Laser Technol., San Diego, CA.* (1963) 63.
4. Carswell, A. Y., *Lidar Measurements of the Atmosphere, Can. J. Phys.* **61** (1983) 378 .
5. Hamilton, P. M., *The Application of a Pulsed-Light Rangefinder (lidar) to the Study of Chimney Plumes, Phil. Trans. R. Soc. London.* **265** (1969) 153.
6. Anfossi, D., P. Bacci and A. Longheto, *An Application of Lidar Technique to the Study of the Nocturnal Radiation Inversion, Atmospheric Environment.* **8** (1972) 537.
7. McElroy, J. L. and M. R. McGown, *Application of Airborne Lidar in Particulate Air Quality Problem Delineation, Monitoring Network Design and Control Strategy Development, Air Waste Manage. Assoc.* **42** (1982) 1186.
8. Menut, L., C. Flamant, J. Pelon and P. H. Flamant, *Urban Boundary Layer Height Determination from Lidar Measurements over the Paris Area, Appl. Optics.* **38** (1999) 954.
9. Di Girolamo, P., P. F. Ambrico, A. Amodeo, A. Boselli, G. Pappalardo and N. Spinelli), *Aerosol Observations by Lidar in the Nocturnal Boundary Layer, Appl. Optics.* **38** (1999) 4585.
10. Bacci, P., G. Elisei and A. Longheto, *Lidar Measurement of Plume Rise and Dispersion at Ostiglia Power Station, Atmospheric Environment* **8** (1974) 1177.
11. Hoff, R.M. and F.A. Froude, *Lidar Observation of Plume Dispersion in Northern Alberta, Atmospheric Environment.* **13** (1979) 35.
12. Whaley, H. and G. K. Lee, *An Assessment of Plume Dispersion Parameters Measured in Fall and Winter at Tar-Sand Refinery Complex, J. Air Pollution Control Assoc.* **28** (6) (1978).
13. McElroy, J. L., *Estimation of Pollutant Transport and Distributions over Complex Terrain of Southern California Using Airborne Lidar, J. Air Pollution Control Assoc.* **37** (1987) 1046.
14. Moore, G. E, L. B. Milich and M. K. Liu, *Plume Behaviors Using Lidar and SF6 Tracer at a Flat and Hilly Site, Atmospheric Environment.* **22** (1988) 1673.
15. Pawlosky, J. N. and D. Iverson, *Use of Optical Remote Sensing Techniques to Monitor Facility Releases, Hydrocarbon Processing.* **77** (1998)125.
16. *U.S. Code of Federal Regulations, Vol. 40, Environmental Protection Agency, Part 60, Appendix A, Alternative Method 1: Determination of the Opacity of Emissions from Stationary Sources Remotely By Lidar, 7-1-95.* **662** (1995).
17. Thomas, G. E, and K. Stamnes, *Radiative Transfer in the Atmosphere and Ocean* (Cambridge University Press, 1999), p. 72.
18. Measures, R. M., *Laser Remote Sensing* (Wiley, New York, 1984).